CORROSION SCIENCE AND TECHNOLOGY, Vol.14, No.6(2015), pp.261~266 pISSN: 1598-6462 / eISSN: 2288-6524
DOI: http://dx.doi.org/10.14773/cst.2015.14.6.261

The Kinetics of Anodic Dissolution and Repassivation on 316L Stainless Steel in Borate Buffer Solution Studied by Abrading Electrode Technique

H. S. Xu[1], D. B. Sun[1], H. Y. Yu[2,†], and H. M. Meng[2]

[1]*National Center for Materials Service Safety (NCMS), University of Science and Technology Beijing, Beijing 100083, China*
[2]*Institute of Advanced Materials and Technology, University of Science and Technology Beijing, Beijing 100083, PR China*
(Received July 29, 2015; Revised November 19, 2015; Accepted November 26, 2015)

The capacity of passive metal to repassivate after film damage determines the development of local corrosion and the resistance to corrosion failures. In this work, the repassivation kinetics of 316L stainless steel (316L SS) was investigated in borate buffer solution (pH 9.1) using a novel abrading electrode technique. The repassivation kinetics was analyzed in terms of the current density flowing from freshly bare 316L SS surface as measured by a potentiostatic method. During the early phase of decay (t < 2 s), according to the Avrami kinetics-based film growth model, the transient current was separated into anodic dissolution (i_{diss}) and film formation (i_{film}) components and analyzed individually. The film reformation rate and thickness were compared according to applied potential. Anodic dissolution initially dominated the repassivation for a short time, and the amount of dissolution increased with increasing applied potential in the passive region. Film growth at higher potentials occurred more rapidly compared to at lower potentials. Increasing the applied potential from 0 V_{SCE} to 0.8 V_{SCE} resulted in a thicker passive film (0.12 to 0.52 nm). If the oxide monolayer covered the entire bare surface (θ=1), the electric field strength through the thin passive film reached 1.6×10^7 V/cm.

Keywords : *repassivation, abrading electrode, anodic dissolution, passive film, high-field model*

1. Introduction

316L stainless steel (SS) is a corrosion-resistant material due to the protection from passive film. However, if the protective oxide film is destroyed chemically or mechanically during service, the breakdown of passivity may result in continuous dissolution from metal substrate, and then severe local corrosion (pitting, SCC, corrosion fatigue et al.) may occurs, even inducing material failure. After the passive oxide film breaking down, the development of corrosion depends on the repassivation kinetics and film structures. A. Kocijan et al. reported on the electrochemical behaviour of 316L SS in borate buffer solutions[1]. Here, 316L SS exhibited anodic peaks in cyclic voltammograms at -0.4 V_{SCE} and 0.6 V_{SCE}, indicating the formation of Fe_2O_3 and the oxidation of Cr(III) to Cr(VI), respectively. The composition and structure of the passive film of stainless steel in high temperature aqueous environment has been instigated[2,3], indicating that the film contains a Cr oxide-rich inner layer and a Fe oxide-rich outer layer. The Mott-Schottky test on 316L SS in borate buffer solution illustrated that the semiconductor properties of passive film changed with potential[4]. Further, the repassivation kinetics has been studied in aqueous environments by mechanical stripping techniques and the results were described by the equation[5,6]:

$$i(t) = A \cdot t^{-\alpha} \tag{1}$$

where $i(t)$ and t represent current density and time respectively. The factor α was the slope determined from log $i(t)$ versus log t plot, which represented repassivation rate and approached to 1[7,8]. It was found that the film initially nucleated and grew according to the place exchange model[9,10], and then grew according to the high electric field ion conduction model, in which log $i(t)$ was linearly proportional to $1/q(t)$, where $q(t)$ was charge density flowing from the bare surface[11-13]. This model assumed that all of current transients only contributed to passive film formation. But without considering anodic dissolution, some investigators pointed out that the linear relationship was breakdown between log $i(t)$ and t at early times of repassivation[14-16].

The goal of this work is to demonstrate the relationship

† Corresponding author: hyyu@ustb.edu.cn

Table 1. Chemical composition of 316L SS (wt.%)

Element	C	Mn	Ni	Cr	Mo	Si	S	P	Fe
wt. %	0.02	1.37	12.2	17.5	2.61	0.68	0.001	0.01	Bal.

between the potentials in passive region and the repassivation kinetics on 316L SS in borate buffer solution. A new type of abrading electrode technique was employed to remove the oxide film on 316L SS. Then current density vs. time curve on bare 316L SS surface was measured by potentiostatic method. Data was analyzed by using an alternative model, which could investigate the kinetics of anodic dissolution and film growth individually. The amount of anodic dissolution and film thickness were discussed, which was expected to substantially advance our understanding of the effect of applied potential on kinetics of dissolution and film formation on 316L SS during repassivation.

2. Experimental Procedure

Material used in this study was type 316L stainless steel and the chemical composition was exhibited in Table 1. The specimens were prepared in the size of 5 mm × 5 mm × 3 mm, and embedded in the centre of epoxy resin with 0.25cm^2 exposure to solution.

A cell was designed to measure the repassivation current on the abraded surface of type 316L SS using a new type of abrading electrode technique, Fig. 1 showed the scheme of the experimental system. Comparing with conventional mechanical stripping techniques, the new method firstly abraded the electrode under protected atmosphere rather than in solution. So the bare electrode surface would keep as film-free surface during abrading. After that the abraded electrode was fast immersed into aqueous solution for current transients recording. Both the two steps were carried out in a sealed chamber with fully filled high purity N_2 (99.999 vol. %), the gas pressure maintained at 0.1 MPa. In order to obtain abraded surface, the electrode surface was push to polish on # 1200 grit SiC abrasive paper. The abrasive paper mounted on a disk plane and fixed to the rotating shaft, which operated by a D.C. motor. The abrading time of specimen was approximately 20 s, and then the abraded electrode surface rotated to parallel with electrolyte level and rapidly immersed into solution within 1-2 ms. The movements of electrode were driven by air pressure cylinders controlled by solenoid valves.

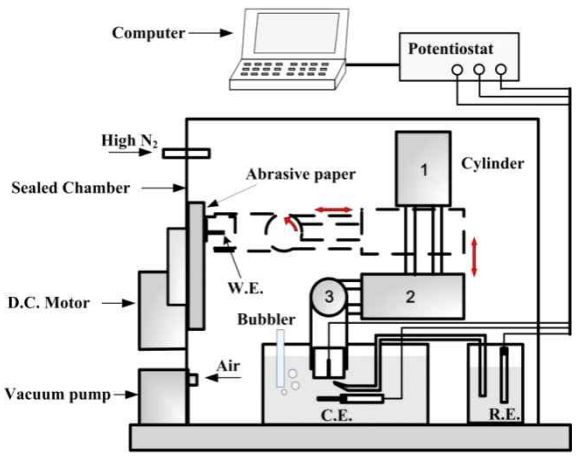

Fig. 1. Schematic diagram of the new type of apparatus for abrading electrode. Dash line in sealed chamber shows the working electrode at its abrading position, and solid line shows the abraded electrode in electrolyte for electrochemical measurement. The translation cylinders (1 and 2) and rotation cylinder (3) drove the working electrode to achieve shifting and rotation.

A saturated calomel electrode (SCE) positioned in a salt bridge with high silica tip and all of electrochemical potentials are referred to the SCE. A large platinum plate was employed as the counter electrode. Gamry Reference 600 Potentiostat was connected to the cell and controlled by Gamry Framework Version 6.21 software. The anodic polarization test of type 316L SS were performed at a potential scan rate of 0.5 mV·s^{-1}. In order to acquire the complete information of repassivation process, the transient current was measured at 1 ms intervals under a potentiostatic condition. All tests were carried out in 25 ℃, 0.05 M H_3BO_3 + 0.075 M $Na_2B_4O_7{\cdot}10H_2O$ borate buffer solution (pH 9.1) deaerated with nitrogen.

3. Results and Discussion

3.1 Polarization measurement

The polarization curve of the 316L SS in Fig. 2 was measured in 0.05 M H_3BO_3 + 0.075 M $Na_2B_4O_7{\cdot}10H_2O$ borate buffer solution at 25 ℃ (pH 9.1). From the polarization curve, the anodic passive region was determined to be from -0.05 V_{SCE} to 0.9 V_{SCE}, at which the current density locates at the magnitudes of 10^{-6} A·cm^2. However, current densities changed suddenly at the potentials of 0 V_{SCE}, 0.2 V_{SCE}, 0.4 V_{SCE}, 0.6 V_{SCE} and 0.8V_{SCE}, as shown in the inset in Fig. 2. It is noteworthy that a bump could be observed at 0.6V_{SCE} during passive region. It might

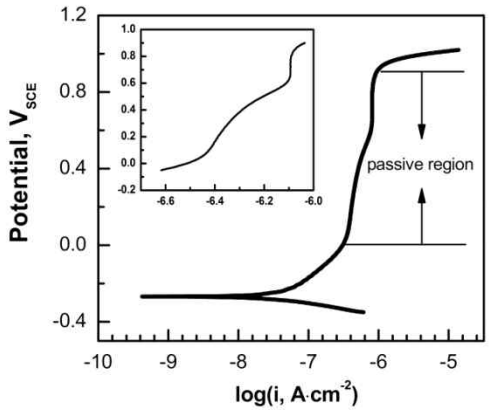

Fig. 2. Polarization curve of 316L SS in 0.05 M H_3BO_3 + 0.075 M $Na_2B_4O_7{\cdot}10H_2O$ borate buffer solution at 25 ℃.

be associated with the reaction of $Cr_2O_3 + 5H_2O = 2CrO_4^{2-} + 10H^+ + 6e$[17].

3.2 Repassivation measurement

Fig. 3 exhibited a typical current decay curve for 316L SS when the abraded surface immersed into a deaerated 0.05 M H_3BO_3 + 0.075 M $Na_2B_4O_7{\cdot}10H_2O$ borate buffer solution at 0 V_{SCE}, 0.2 V_{SCE}, 0.4 V_{SCE}, 0.6 V_{SCE} and 0.8 V_{SCE}. The peak value increased with applying higher potential. Once the abraded electrode contacted the solution, the anodic current flowing through the abraded surface raised abruptly to a peak due to an anodic oxidation reaction, in which the stabilization of potential on abraded electrode occurred, thereafter decayed as the repassivation proceeded.

Based on the data in Fig. 3 and taking 0 V_{SCE} as an example, the relationship between log $i(t)$ and log t was draw according to Eq. 1 in Fig. 4. It was obviously seen that a depassivation time was approximately 100 ms, obtaining a more or less horizontal slop. And then a steady linear slop of approximately -1.24 was obtained within 2 s. And the slop should be less than 1 according to the high-field ion conduction model[18]. Therefore, the slope of the log-log plot deviated from the high field behaviour, because anodic dissolution of bare electrode surface was neglected in current analysis. But the anodic dissolution on abraded electrode might partially contribute to the total current. It would delay the current decay and increase the slope of log i vs. log t in the initial stage of repassivation. With film thickening, the electric field in film gradually reduced, which slowed down the transportation rate for cations through the film. Hence the repassivation rate decreased after 2 s until reaching a steady state.

3.3 Current transients analysis

In order to analyze the repassivation kinetics based on the viewpoint that the current from the abraded surface is not only from film formation but also from anodic dissolution in the initial stage. We employed an alterable mathematical expression to fit current decay transients, which proposed by Lillard[14],

$$I_{tot} = I_{diss} + I_{film} = (1-\theta)\cdot I_{bare} + \theta A t^{-b} \qquad (2)$$

where I_{bare} was the bare surface current, here it equaled to peak current. A was a characteristic charge density coefficient, and b was a constant, θ represented the fraction of the bare surface that was covered by a passivating film, which derived from Avrami kinetics[19],

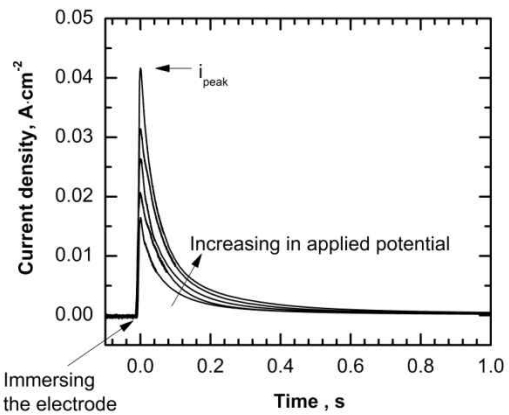

Fig. 3. Current transients curve for 316L SS in deaerated borate buffer solution at different applied potentials.

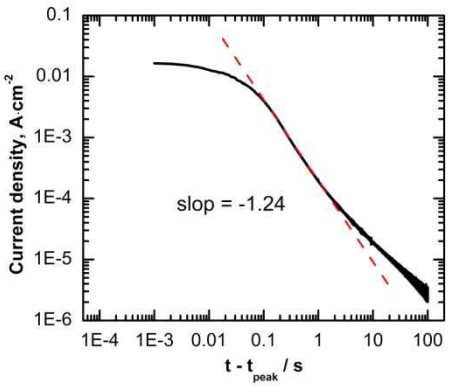

Fig. 4. log $i(t)$ vs. log t curve in deaerated borate buffer solution at the applied potential of 0 V_{SCE}.

$$\theta = 1 - \exp(-kt^n) \quad (3)$$

where k was the film formation rate and n was the exponent related to the geometry of the film growth. This model provided us an approach to investigate the kinetics of dissolution and repassivation on the bare surface of metal.

Current decay curves in borate buffer solution under different potentials were fitted to this model in attempt to separate the current into dissolution and film formation components at early times after electrode immersion. The geometrical parameter n was fixed at 1 and current density was used instead of current. The data before current peak had not been fit this model, in which the constant applied potential did not reach a steady state on bare 316L SS surface in solution. This is because the model was based on an assumption that film would grow with time on bare electrode surface, and the anodic dissolution will stop dominating after a relatively short time. The current decay curves of 316L SS in borate buffer solution under 0V_{SCE} were fit by using Eq. (3) and Eq. (4), and the fitting result was presented in Fig. 4. When applied potentials at 0.2 V_{SCE}, 0.4 V_{SCE}, 0.6 V_{SCE}, 0.8 V_{SCE}, the current transients were also be fitted. The model was good agreement with the experiment data ($R^2 > 0.98$) and corresponding parameters were listed in Table 2.

From the fit parameters, we calculated i_{diss} and i_{film} and θ as a function of time, as shown in Fig. 5. Before i_{diss} equaled to i_{film}, metal anodic dissolution dominated the

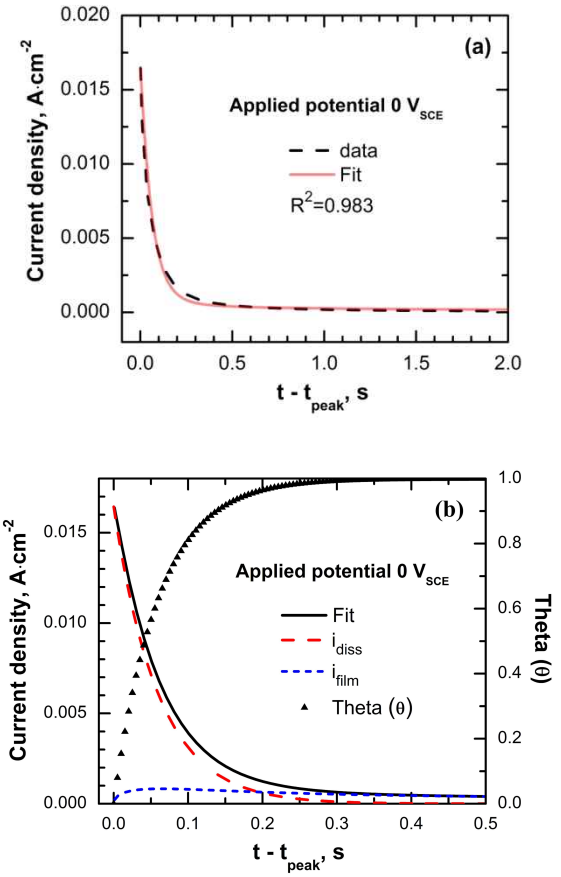

Fig. 5. (a) Fits of Eq. (2) to current transients for 316L SS in borate buffer solution at 0 V_{SCE}; (b) dissolution and film growth currents as a function of time as well as the fraction of surface coverage were calculated from the fit parameters.

Table 2. Average fit parameters and standard deviation for 316L SS in 0.05 M H_3BO_3 + 0.075 M $Na_2B_4O_7 \cdot 10H_2O$ borate buffer solution from Eq. (4) and Eq. (5)

Applied potential, V_{SCE}	k, s^{-1}	A, $\times 10^{-4}$ C·cm^{-2}	b
0	16.61±0.89	2.71±0.47	0.56±0.03
0.2	17.66±1.05	4.37±0.62	0.64±0.08
0.4	16.84±1.52	6.41±0.72	0.42±0.05
0.6	15.37±1.19	7.26±0.73	0.49±0.07
0.8	19.95+1.87	8.65±1.45	0.65±0.09

Table 3. Time of i_{diss}=i_{film} and θ =1, calculated values of dissolution charge density and dissolution vertical depth for 316L SS in 0.05 M H_3BO_3 + 0.075 M $Na_2B_4O_7 \cdot 10H_2O$ borate buffer solution

Applied potential, V_{SCE}	$t(i_{diss} = i_{film})$, s	$t(\theta = 1)^a$, s	q_{diss}, mC·cm^{-2}	h_{diss}, nm
0	0.18	0.42	0.97	0.24
0.2	0.15	0.39	1.15	0.28
0.4	0.18	0.41	1.54	0.37
0.6	0.20	0.45	2.01	0.49
0.8	0.13	0.35	2.05	0.50

Note: [a]Given the logarithmic behavior of θ a value of 0.9999 is used for consistency and not 1.

process in repassivation, and then the i_{diss} fell below i_{film} and gradually reached 0 at θ = 1. As applied potential at 0 V_{SCE}, the times for $i_{diss} = i_{film}$ and $\theta = 1$ were 0.18 s and 0.42 s, respectively. Approximately 0.97 mC·cm^{-2} of charge density (q_{diss}) was consumed for anodic dissolution from the current peak to $\theta = 1$. Assuming metal dissolved uniformly from the abraded surface, using the equivalent weight (56.18 g·mol^{-1}) and density (7.99 g·cm^{-3}) for 316L SS passive film[20], the corresponding vertical depth (h_{diss}) for dissolution was approximately 0.24 nm. The results under other applied potential were compared in Table 3. The repassivation processes at different potentials were dominated by anodic dissolution in the initial stage, but the dissolution current rapidly decayed, and the dissolution charge density and vertical depth for dissolution from 316L SS surface increased with applied potential increasing from 0 to 0.8 V_{SCE}.

3.4 Film thickness calculation

As commented above, the calculated film formation current densities (i_{film}) as a function of time were consumed to establish passivity on the abraded electrode surface, as shown in Fig. 5. To examine differences in film thickness as a function of applied potential, we calculated the film formation charge density $q(t)$ by integrating i_{film} as a function of time:

$$q_{film}(t) = \int_{t=0}^{t} i_{film} d(t) \tag{4}$$

and $q(t)$ followed the relationship with the film thickness $h(t)$, given by Faraday's Law:

$$q_{film}(t) = h(t) \cdot zF\rho / M \tag{5}$$

where z was the number of electrons transferred for cations, F was the Faraday constant (96485.34 C·mol^{-1}), M was the molecular weight of the film, ρ was the density of film. The passive film formed on stainless steel in aqueous is predominantly a Cr(III) rich oxide film, which have been reported by some investigators[21-23], $z = 3$, $M = 152$ g·mol^{-1} and $\rho = 5.2$ g·cm^{-3}.

Assuming the oxide nucleated at constant thickness, the charges transferring through electrode surface would be consumed to form a monolayer before the time of $\theta = 1$. After that, the charges were consumed as film thickening. Consequently, The film growth as a function with time from the time of $\theta = 1$ also was calculated and presented in Fig. 6. The incipient at $\theta = 1$ represented thickness of monolayer. It was noted that film thickness changes linearly with time.

As it was expected, the higher the applied potential, the higher the total charge density consumed in the passive film formation and the thicker the new passive film formed on the abraded surface, except for the test at 0.2 V_{SCE}, where the charge density involved in the repassivation process was slightly higher than at 0.4 V_{SCE}, although the difference was not significant. The fitting results of the linear relationship between film growth and time were presented in Fig. 6, it seemed that the growth rate increased with the potential from 0 V_{SCE} to 0.8 V_{SCE}, while it appeared similar at 0.2 V_{SCE}, 0.4 V_{SCE} and 0.6 V_{SCE}.

The incipient film thickness h_m (Fig. 4, $h(t)$ at $\theta = 1$), was plotted as a function of applied potential in Fig. 7. The change in thickness appeared to be linear with applied potential, indicating constant electric field strength for passive film growth on 316L SS in borate buffer solution. A linear slope (0.61 nm·V^{-1}) was obtained from Fig. 7. Converting to cm and taking the inverse of the value, the

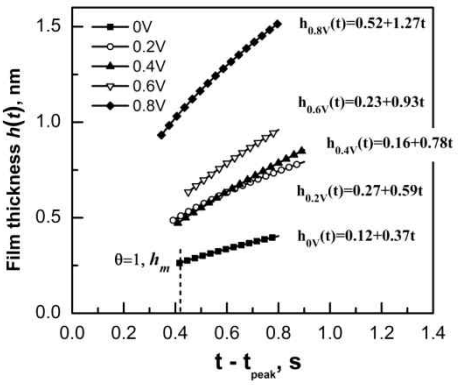

Fig. 6. Oxide film thickness as a function with time from $t(\theta=1)$ on 316L SS surface in borate buffer solution at 0, 0.2, 0.4, 0.6 and 0.8 V_{SCE}.

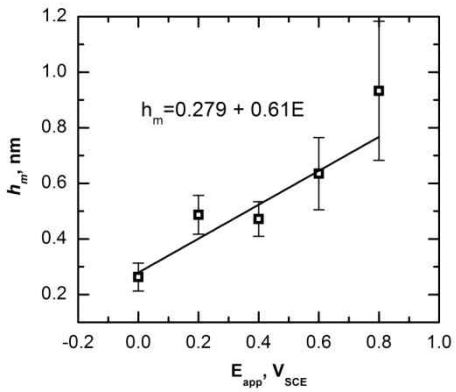

Fig. 7. The average oxide film thickness of monolayer at θ=1, as a function of applied potential.

calculated electric field strength of the incipient films was 1.64×10^7 V·cm^{-1}. This magnitude of electric field strength was consistent with the high electric field ions conduction model, in which a high electric filed assisted cation to transfer through film. The film grew according to high-field model from the time of $\theta = 1$. However, the rise of film thickness would result in the decline of the electric field strength; hence the film growth rate decreased gradually and formed a steady passive film at last.

4. Conclusions or Summary

(1) The high electric field ions conduction model was breakdown for the initial repassivation analysis of 316L SS in borate buffer solution. The current transients of repassivation were fit with an alternative model to analyze the kinetics of anodic dissolution and film formation individually.

(2) The repassivation process of 316L SS in borate buffer solution was dominated by anodic dissolution in the initial repassivation. As applied potential increasing from 0 V_{SCE} to 0.8 V_{SCE}, the dissolution charge density increased and dissolution vertical depth changed from 0.24 nm to 0.5 nm.

(3) The film thickness of 316L SS in borate buffer solution was calculated by Faraday's Law. Higher applied potentials resulted in more current densities consuming for film growth and thicker monolayer formed. The film grew linearly with time and the growth rate increased as the applied potential from 0 V_{SCE} to 0.8 V_{SCE}.

(4) From the plot of film thickness vs. potential the electric field strength for 316L SS film growth in borate buffer solution was found to be 1.64×10^7 V·cm^{-1}. It seemed that the oxide film was thickening by high electric field ions conduction mechanism after the surface covered by monolayer.

Acknowledgments

This work was supported by China National Natural Science Foundation (51371033), and the Specialized Research Fund for the Doctoral Program of Higher Education of China (20130006110034).

References

1. A. Kocijan, Č. Donik, M. Jenko. *Corros. Sci.*, **49**, 2083 (2007).
2. S. E. Ziemniak, M. Hanson, *Corros. Sci.*, **44**, 2209 (2002).
3. D. Shintani, T. Ishida, H. Izumi, et al., *Corros. Sci.*, **50**, 2840 (2008).
4. H. H. Ge, X. M. Xu, L. Zhao, et al., *J. Appl. Electrochem.*, **41**, 519 (2011).
5. P. Engseth, J. C. Scully, *Corros. Sci.*, **15**, 505 (1975).
6. Jae-Bong Lee, *Mater. Chem. Phys.*, **99**, 224 (2006).
7. P. Engseth, J. C. Scully, *Corros. Sci.*, **15**, 505 (1975).
8. F. M. Song, K. S. Raja, D. A. Jones, *Corros. Sci.*, **48**, 285 (2006).
9. Norio Sato, Morris Cohen, *J. Electrochem. Soc.*, **111**, 512 (1964).
10. Eun-Ae Cho, Chin-Kwan Kim, Joon-Shick Kim, Hyuk-Sang Kwon, *Electrochim. Acta*, **45**, 1933 (2000).
11. N. Cabrera, N. F. Mott, *Rep. Prog. Phys.*, **12**, 163 (1948).
12. G. T. Burstein, P. I. Marshall, *Corros. Sci.*, **23**, 125 (1983).
13. H. S. Kwon, E. A. Cho, and K. A. Yeom, *Corrosion*, **56**, 32 (2000).
14. R. S. Lillard, G. Vasquez Jr., D. F. Bahr, *J. Electrochem. Soc.*, **158**, C194 (2011).
15. R. M. Fernández-Domene, E. Blasco-Tamarit, D. M. García-García, J. García-Antón, *Electrochim. Acta*, **58**, 264 (2011).
16. Lindsey R. Goodman, Preet M. Singh, *Corros. Sci.*, **65**, 238 (2012).
17. M. Gojic, D. Marijan, L. Kosec, *Corrosion*, **56**,839 (2000).
18. G. T. Burstein, A. J. Davenport, *J. Electrochem. Soc.*, **136**, 936 (1989).
19. M. Avrami, *J. Chem. Phys.*, 7, 1103 (1939).
20. Z. Feng, X. Cheng, C. Dong, et al., *Corros. Sci.*, 52, 3646 (2010).
21. L. J. Oblonsky, M. P. Ryan, and H. S. Isaacs, *J. Electrochem. Soc.*, **145**, 1922 (1998).
22. J. Doff, P. E. Archibong, G. Jones, *Electrochim. Acta*, **56**, 3225 (2011).
23. H. P. Leckie and H. H. Uhlig, *J. Electrochem Soc.*, **113**, 1262 (1966).